Mechanism of Calcium Incorporation Inside Sol–Gel Silicate Bioactive Glass and the Advantage of Using Ca(OH)2 over Other Calcium Sources

C. Bossard, Henri Granel, E. Jallot, V. Montouillout, F. Fayon, J. Soulie, C. Drouet, Y. Wittrant, J. Lao

Mechanism of Calcium Incorporation Inside Sol–Gel Silicate Bioactive Glass and the Advantage of Using $Ca(OH)_2$ over Other Calcium Sources

Cédric Bossard,[*,†] Henri Granel,[‡] Édouard Jallot,[†] Valérie Montouillout,[§] Franck Fayon,[§] Jérémy Soulié,[∥] Christophe Drouet,[∥] Yohann Wittrant,[‡] and Jonathan Lao[†]

[†]Université Clermont Auvergne, CNRS/IN2P3, Laboratoire de Physique de Clermont, BP 10448, F 63000 Clermont Ferrand, France

[‡]Unité de Nutrition Humaine, Université Clermont Auvergne, INRA, UNH, CRNH Auvergne, F 63000 Clermont Ferrand, France

[§]CNRS, CEMHTI UPR3079, Université d'Orléans, 1D avenue de la Recherche Scientifique, 45071 Orléans, France

[∥]CIRIMAT, Université de Toulouse, CNRS/INPT/UPS, Ensiacet, 4 Allée Emile Monso, 31030 Toulouse Cedex 4, France

ABSTRACT: Calcium is an essential component of osteogenesis and is often required for imparting significant bioactivity to synthetic bone substitutes and, in particular, silicate based materials. However, the mechanism of calcium incorporation inside sol–gel silicates is poorly understood. In this work, we shed light on the determinant parameters for incorporation of calcium into acid–base catalyzed sol–gel silicates at ambient temperature: increasing the pH above the isoelectric point of silicic acid and the nature of the calcium counterion in the calcium precursor are found to be the key. Based on our proposed reaction sequence, we were able to compare calcium precursors and select an ideal candidate compound for the synthesis of bioactive glasses (BG) and organic–inorganic hybrids at ambient temperature. Reproducible syntheses and gel times of SiO_2–CaO BG were obtained using calcium hydroxide (CH), and we demonstrate its usability in the synthesis of promising BG–polycaprolactone hybrid scaffolds. BG and hybrids prepared with CH were able to form nanocrystalline nonstoichiometric apatite in simulated body fluid. The increased reliability of low temperature syntheses associated with the use of a stable and inexpensive alkaline earth precursor are major steps toward the translation of calcium silicate hybrids or other alkaline earth silicates from bench to clinic.

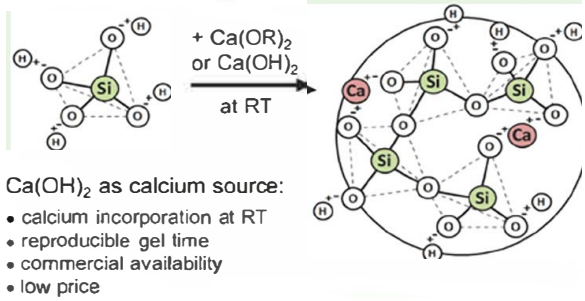

KEYWORDS: *bioactive glass, calcium incorporation, apatite identification, polycaprolactone, hybrid, scaffold*

1. INTRODUCTION

Since they were first developed by Hench in 1969,[1] bioactive glass (BG) have been the focus of much research due to their remarkable properties: they strongly bond to bone,[2] they resorb as bone regenerates, and their dissolution products stimulate osteoblasts at the genetic level.[3] BG can be fabricated in various shapes such as monoliths, particulates, and scaffolds. However, their inherent brittleness prevents BG scaffolds from being viable in cyclic load bearing applications.[4] The toughness of the material can be greatly enhanced by combining BG with a polymer to produce a composite or an organic–inorganic sol–gel hybrid. Unlike conventional composites, BG–polymer sol–gel hybrids behave as a single phase thanks to the interpenetration of the organic and inorganic networks at a molecular level.[5] Another key advantage of these hybrids is the potential for tailoring their degradation rates and their mechanical properties through a controlled covalent linkage between the organic and inorganic chains.[6−8]

Even though BG–polymer hybrid scaffolds appear as promising bone substitutes, their development is hindered by the difficulty of incorporating calcium ions into the BG silicate network. Calcium plays a central role in the bioactivity of BG[9] and its release is known to favor the adsorption of proteins involved in osteogenic processes and inflammatory response,[10] and to induce osteoblast proliferation and differentiation.[11] Traditionally, sol–gel BG are prepared from salts like $CaCl_2$ or $Ca(NO_3)_2$, but these calcium sources require a thermal treatment above 400 °C to allow calcium to enter the silicate network and to remove the counterion, as this has been well established in pioneering works by Lin, Yu, and Jones et al.[12,13] In the synthesis of hybrids, the presence of a polymer at an early stage of the sol–gel process forbids such thermal treatments; as a consequence, hybrids prepared from calcium salts are likely made of a pure silica–polymer hybrid in which the silicate network is coated with these salts.[14−16] This superficial calcium deposit is likely to be washed out at the first contact with body fluids, thus causing a substantial burst increase in calcium concentration[17] that may lead to

DOI: 10.1021/acsbiomaterials.9b01245

cytotoxicity. In contrast, the use of calcium alkoxides ($Ca(OR)_2$, where R is an alkyl group) as sol−gel precursors allows calcium incorporation at room temperature.[13] BG−polymer hybrids with well incorporated calcium were obtained from calcium methoxyethoxide[18−20] or calcium ethoxide (CE).[21−23] Nevertheless, all the authors reported a rapid gelation of the sol when using these alkoxides. The gelation was even faster in the presence of water, which is commonly employed to produce scaffolds by sol−gel foaming.[24] The premature gelation associated with calcium alkoxides makes it challenging to handle and process the unstable sol to generate a macroporous structure and might explain why hybrids were mainly fabricated in the form of fiber[18] or dense[19,20] materials. In previous works, we successfully developed a protocol that allows the syntheses of hybrid scaffolds using CE.[21−23] The gelation of the hybrid sol was delayed to several hours by using a reduced water to tetraethylorthosilicate (TEOS) molar ratio of 2 under dilute conditions. Although hybrid scaffolds with well incorporated calcium were produced in a relatively simple manner, the gelation time was found to be highly dependent on the origin (supplier, batch) and the age of the calcium precursor as alkoxides are sensitive to moisture. These inconsistencies may constitute a major issue when translating these materials from bench to clinic since synthesis processes have to be reliable and reproducible to obtain regulatory approval and satisfy industrial demand. Finally, calcium alkoxides are expensive and not always available for purchase due to limited stocks and suppliers.

Obviously, these facts evidence our poor understanding of how the calcium source influences the chemistry of silicate species during the sol−gel synthesis. To date, only partial explanations are found in the literature. The aim of this work is to improve the comprehension of mechanisms of calcium incorporation inside sol−gel silicates to identify reliable calcium precursors that allow calcium incorporation under reproducible syntheses conducted at room temperature. The latter point is key for the synthesis of organic−inorganic hybrids. We investigate and compare the behavior of calcium salts and alkoxides under syntheses conducted in similar conditions, as opposed to the varying conditions found in the literature that make it difficult to draw a conclusion, and explore the use of one of the most abundant and inexpensive sources of calcium: calcium hydroxide (CH). Depending on the sources, calcium incorporation in SiO_2−CaO BG is examined and, when appropriate, their usability and introduction in the synthesis of organic−inorganic hybrid scaffolds consisting of BG and polycaprolactone (PCL) are evaluated. The in vitro apatite forming ability and cytotoxicity of selected candidates are discussed.

2. MATERIALS AND METHODS

2.1. Synthesis. BG with a composition of 75 wt % SiO_2−25 wt % CaO were produced from tetraethylorthosilicate (TEOS) (99% purity, Aldrich) and either $CaCl_2$ (96% purity, Sigma Aldrich), tricalcium dicitrate tetrahydrate (99% purity, Aldrich), calcium acetate monohydrate (99% purity, Sigma Aldrich), CE ($Ca(OC_2H_5)_2$, 95% purity, Gelest), or CH ($Ca(OH)_2$, 98% purity, Acros Organics). TEOS was first hydrolyzed in ethanol (absolute, VWR Chemicals) by adding 2 M HCl (obtained from 37% fuming, Aldrich) (molar ratio EtOH/H_2O/TEOS/HCl = 3.7:2:1:0.07). The same volume of ethanol was used for the dissolution (or partial dissolution) of the calcium source and the two solutions were mixed together to obtain a sol that was left for condensation. When employing calcium citrate or $CaCl_2$ as the calcium source, a solution of saturated sodium hydroxide (NaOH, 97% purity, Sigma Aldrich) in ethanol was added dropwise to increase the pH of the sol and obtain a similar pH value to that of the CE or CH sols. After gelation, BG were kept for 72 h in a sealed flask for aging, and then they were dried at room temperature. Finally, BG were ground into fine powders prior to analysis.

Hybrids comprised of 70 wt % PCL−30 wt % BG were produced by mixing a solution of PCL (M_n = 80 000 g mol^{-1}, Aldrich) dissolved in tetrahydrofuran (99.9% purity, Sigma Aldrich) (18.2 w/v %) with the BG sol right before its gelation. The hybrid sol was stirred for 1 h for homogenization and further condensation, and then it was processed into scaffolds thanks to a porogen leaching method that was described in a previous work.[22] Briefly, 400−600 μm paraffin spheres were stacked in a mold and heated at 50 °C for 60 min to partially fuse them. The BG−PCL hybrid sol was infiltrated into the stack of microspheres by centrifugation and left for gelation (72 h). The obtained material was immersed in cyclohexane (99.99% purity, Fisher Chemical) baths until the complete dissolution of the paraffin porogen. Finally, the macroporous hybrid scaffold was rinsed in absolute ethanol and dried at room temperature.

Some calcium phosphate compounds were used in this work as reference materials. Stoichiometric hydroxyapatite was obtained via dropwise addition under reflux of a solution of diammonium hydrogen phosphate into a boiling solution of calcium nitrate, in stoichiometric proportions, and in the presence of ammonia to retain alkaline conditions (close to pH 10). Decarbonated water, previously boiled, was used to avoid carbonation contamination. After 4 h of aging, the precipitate was filtered, washed with DI water, dried at 100 °C, and calcined at 1000 °C for 1 h.

The biomimetic nanocrystalline apatite sample used in this study was prepared by double decomposition from aqueous solutions of diammonium hydrogen phosphate in excess (0.6 M) and calcium nitrate (0.3 M) at room temperature ($T \sim 22$ °C) and initial pH ~ 7.2 provided by the excess of phosphate ions acting as an internal buffer agent. After rapid mixing (1 min), the precipitate was aged in solution for 1 day and then filtered, washed, and freeze dried. Typical physicochemical features for this sample can be found elsewhere.[25]

Octacalcium phosphate $Ca_8(PO_4)_4(HPO_4)_2{\cdot}5H_2O$ was precipitated by hydrolysis, under stirring, of brushite crystals in the presence of an identical weight of diammonium hydrogen phosphate at 37 °C for 24 h. The precipitate was then filtered, washed, and freeze dried.

2.2. Evaluation of Apatite-Forming Ability. Simulated body fluid (SBF) was prepared following Bohner and Lemaitre's recommendations.[26] BG powders and BG−PCL hybrid scaffolds were immersed in SBF at a ratio of 1 mg mL^{-1} and put on an orbital shaker with an agitation rate of 250 rpm at 37 °C. The scaffolds were glued to the bottom of the flasks to prevent them from floating and placed under vacuum for 5 min to ensure the infiltration of SBF in the pores. After 6 h, 1 day, 3 days, and 7 days of interaction, the solutions were filtered with a 0.2 μm paper and the Si, Ca, and P concentrations were determined by inductively coupled plasma atomic emission spectroscopy (ICP AES) (n = 3). The materials were rinsed with absolute ethanol to avoid further mineralization and dried at ambient temperature.

2.3. Solid-State Nuclear Magnetic Resonance (NMR) Spectroscopy. All solid state NMR experiments were performed on a Bruker Avance I spectrometer operating at a magnetic field of 9.4 T (^{1}H, ^{29}Si, and ^{31}P Larmor frequencies of 400.2, 79.5, and 162.0 MHz) using a 4 mm double resonance MAS probehead. ^{1}H SPINAL 64 decoupling[27] with a nutation frequency of 70 kHz was applied during signal acquisition. The ^{29}Si quantitative MAS spectra were recorded at a spinning frequency of 10 kHz with a pulse duration of 2.4 μs (corresponding to a flip angle of 30°) and a recycle delay of 10 s. ^{31}P quantitative MAS spectrum was recorded at a spinning frequency of 14 kHz with a pulse duration of 1.75 μs (corresponding to a flip angle of 20°) and a recycle delay of 30 s. ^{29}Si and ^{31}P chemical shifts were referenced relative to tetramethylsilane and H_3PO_4. The spectra were simulated using DMfit software.[28] The degree of condensation (DC) was calculated using the following equation

$$DC = 100 \times \frac{2 \times (Q^2_{Ca/H} + Q^2_{2H}) + 3 \times (Q^3_{Ca} + Q^3_{H}) + 4 \times Q^4}{4} \quad (1)$$

2.4. X-ray Diffraction (XRD). Prior to analysis, the CH source and BG were crushed into fine powders, BG−PCL hybrid scaffolds were sliced into small granules with a knife mill, while pure PCL was processed into a membrane by solvent casting. XRD analysis was performed using an Equinox 100 diffractometer (INEL) equipped with a cobalt anticathode (λ = 1.78892 Å). The whole 2θ range was measured simultaneously thanks to a curved detector. Each sample was analyzed for 2 h.

2.5. Fourier Transformed Infrared (FTIR) Spectroscopy. FTIR spectroscopy was performed in the mid IR domain (400−4000 cm^{-1}) using a Thermo Fischer Scientific spectrometer (IS 50 FTIR model) in the attenuated total reflectance (ATR) mode using a diamond crystal or in the transmission mode for better assessing the 400−600 cm^{-1} spectral range. Transmission FTIR spectra were obtained using the KBr pellet method. During the preparation of KBr pellets, however, BG−PCL hybrid scaffolds could not be thinly ground because of their plasticity; hence, they were simply crushed into pieces using a mortar and dispersed in the KBr powder. Likewise, pure PCL membrane was cut into pieces using a scalpel. The number of scans was set to 64 in the ATR mode and 128 in the transmission mode, with a spectral resolution of 4 cm^{-1}.

2.6. Scanning Electron Microscopy (SEM). The macroporous structure of BG−PCL hybrid scaffolds was observed with an SH 3000 SEM (Hirox) at 10 keV; prior to analysis, the samples were coated with carbon using vacuum sputtering. After interaction with SBF, the surface of BG−PCL hybrid scaffolds was observed with an FEI Quanta 450 SEM microscope at 15 keV under low vacuum (80 Pa); prior to analysis, the samples were coated with silver using physical vapor deposition.

2.7. In Vitro Biocompatibility. *2.7.1. Cell Culture.* Primary osteoblasts were isolated from 3 day old rats according to Declercq et al.[29] Briefly, calvaria were dissected and cells were extracted through different enzymatic digestions (collagenase IA and dispase II) at 37 °C. Cells were washed and then cultivated in the culture medium that consisted of Minimum Essential Medium Eagle α Modifications supplemented with 10% fetal bovine serum and 1% penicillin/streptomycin. The cell culture was carried out at 37 °C, 5% CO_2, and 90% hygrometry until 80% confluency before cell seeding.

2.7.2. Cell Viability. The biocompatibility of the BG−PCL hybrid scaffolds was evaluated in vitro by an indirect cytotoxicity assay. To do so, BG−PCL hybrid scaffolds (n = 3) were placed in cell culture inserts equipped with a membrane with a pore size of 8 μm (Falcon) and the inserts were fixed in a 12 well plate. Scaffolds were first incubated in the culture medium (0.07 mL per mg of material) for 72 h as recommended by Midha et al. (preconditioning step).[30] After removing the medium, primary osteoblasts (p + 1) dispersed in a specific volume of fresh culture medium (0.07 mL per mg of material) were seeded onto the well plate to reach a density of 10 000 cells per cm^2. The culture was carried out for 6 days. The culture medium was renewed every two days. Finally, cell viability was determined by an XTT based method using the Cell Viability/Proliferation Kit II (Sigma Aldrich) according to the recommendations of the supplier. The optical density was determined at 450 nm and the results were normalized with respect to the control condition in which no biomaterial was employed. Differences between the samples were estimated using Tukey's HSD post hoc test (significance level was set to 0.05).

3. RESULTS AND DISCUSSION

3.1. Influence of the pH. *3.1.1. On the Gel Time.* The mechanism of calcium incorporation into the silicate network during the sol−gel process remains unclear. When using calcium alkoxides, it is generally assumed that they are highly reactive toward water and quickly undergo hydrolysis and condensation, thus provoking a rapid gelation of the BG sol.[5,13,18,19,21,22] Surprisingly, the basic property of alkaline earth metal alkoxides has barely been considered to explain the rapid gelation associated with the introduction of calcium alkoxide in the sol.[31] Yet, the pH is known to greatly alter the chemistry of silanol species and influence the gel time of silica.[32]

To evaluate the impact of the pH on the gel time, we carried out several syntheses. After introducing CE to a sol of previously acid catalyzed hydrolyzed TEOS, the pH rose from 0 to 5 and the gelation happened 2 h 40 min later. For comparison, the pH of an identical sol of prehydrolyzed acid catalyzed TEOS was adjusted to 5 by adding a solution of sodium hydroxide. The sol gelled in 1 h 30 min. If the pH is left unmodified (pH = 0, no NaOH added), the sol remains liquid and does not polymerize after an entire week. Therefore, the quickened gelation observed with calcium alkoxides is not likely caused by their reactivity toward water, but rather by the pH increase associated with their basic property.

The accelerated gelation of aqueous silicate sols was also observed when adding metal salts in acid catalyzed sols of hydrolyzed TEOS. Yu et al. reported a rapid gelation with calcium acetate (pK_a = 4.8) compared to the neutral salts $Ca(NO_3)_2$ and $CaCl_2$.[13] Likewise, Maçon et al. reported a gel time of 1 h with lithium citrate (pK_{a1} = 3.1, pK_{a2} = 4.8, pK_{a3} = 6.4) associated with a pH increase from 1 to 5.3, whereas the sol remained at pH < 2 when using the neutral $LiNO_3$ salt and gelled in 3 days.[33] This clearly shows an existing relationship between the gel time and the rise of the pH above the IEP of silicic acid (around pH = 2 in aqueous media)[34] caused by the introduction of the calcium precursor, which is not exclusive to calcium alkoxides.

3.1.2. On Calcium Incorporation. Although pH appears to be a major parameter with regard to the condensation rate of silicate species, it is not clear whether it plays a role in the incorporation of calcium ions into the silicate network. In the literature, pH is rarely taken into account: studies showed that calcium is incorporated when employing calcium alkoxides (presumably at pH > 2),[13,18−21] while it is not when employing $CaCl_2$ or $Ca(NO_3)_2$ (presumably at pH < 2).[13,19] As the pH is varied, it is difficult to conclude whether calcium incorporation is governed solely by the nature of the calcium source. Some authors suggested the possible influence of pH on calcium incorporation.[12,31,35,36] The hypothesis is that protonated silanols (SiOH) are predominant below the IEP of silicic acid, whereas above the IEP of silicic acid, deprotonated silanols (SiO^-) act as weak chelators for metallic ions and allow the formation of $SiO^-\ ^+Ca$ bonds.

Here, to investigate the possible impact of the pH on calcium incorporation, BG composed of 75 wt % SiO_2−25 wt % CaO were produced using CE (BG−CE), CH (BG−CH), $CaCl_2$ (BG−CCl), calcium citrate (BG−CCit), or calcium acetate (BG−CAc) as calcium precursors following sol−gel processes conducted at a similar pH (Table 1). After the prehydrolysis of TEOS under acidic conditions, the calcium source was introduced in the sol. The pH spontaneously rose to 1 for BG−CCit due to the weak basicity of citrate anions and to 5 for BG−CE and BG−CH due to the strong basicity of ethoxide and hydroxide anions, respectively. For BG−CCl and BG−CCit, it was therefore necessary to add sodium hydroxide to reach pH = 5. The BG sols gelled in 2 h 40 min (BG−CE), 1 h 30 min (BG−CH, BG−CCl), and 30 min (BG−CCit). The faster gelation of the BG−CH and BG−CCl sols compared to the BG−CE sol is explained by the in

Table 1. Summary of the Conditions used to Synthesize SiO_2−CaO BG from Different Calcium Precursors

condition name	acid-catalyzed sol of hydrolyzed TEOS	pH	gelation time (h)
BG CE	+ calcium ethoxide	5	1.5 2.7
BG CH	+ calcium hydroxide	5	1.5
BG CCl	+ calcium chloride + NaOH (to increase pH)	5	1.5
BG CCit	+ calcium citrate + NaOH (to increase pH)	5	0.5
BG CAc	+ calcium acetate	5	heterogeneous

situ generation of water resulting from the neutralization reaction between the HCl catalyst and the CH or NaOH base. Indeed, the amount of water is known to influence the gel time of silicate sols,[34,37] especially since a reduced water to TEOS ratio of 2 was employed here. For BG−CCit, the gelation of the sol was even faster owing to the hydrated nature of the calcium precursor (tricalcium dicitrate tetrahydrate). Regarding calcium acetate, its introduction led to a spontaneous pH increase to 5, but the BG−CAc sol gelled heterogeneously, which is attributed to the presence of acetic acid as we obtain a similar result when adding acetic acid in a BG−CE sol. As such, calcium acetate does not seem to fit our synthesis conditions and was not further studied, although it might be useful in sol−gel syntheses that successfully employ acetic acid as a catalyst.[38,39]

After aging and drying, the resultant glasses were analyzed by ^{29}Si MAS NMR spectroscopy to investigate calcium incorporation (Figure 1). The presence of Q^3_{Ca} (−93.0 ppm)

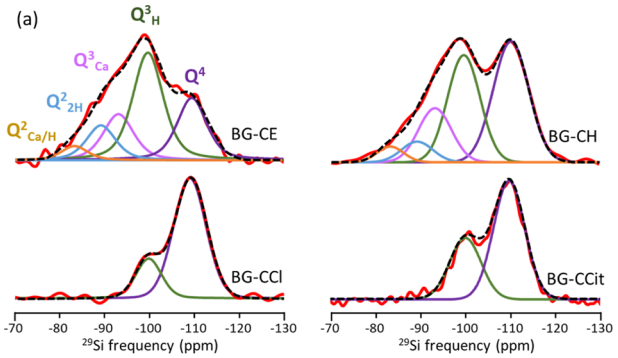

(b)

	Intensity (%)					DC (%)
	$Q^2_{Ca/H}$	Q^2_{2H}	Q^3_{Ca}	Q^3_H	Q^4	
BG-CE	4	12	18	40	26	78
BG-CH	4	6	17	33	40	83
BG-CCl	0	0	0	22	78	95
BG-CCit	0	0	0	34	66	92

Figure 1. (a) Experimental solid state ^{29}Si MAS NMR spectra (red lines) of SiO_2−CaO BG glasses obtained using different calcium precursors and their fits (black dots). Individual Q^n contributions are shown below each experimental spectrum. (b) Relative intensities of Q^n resonances obtained from fits and degrees of condensation (DC).

and $Q^2_{Ca/H}$ (−83.0 ppm) species is considered a signature of the incorporation of calcium ions into the silicate network and is observed for BG−CE and BG−CH (Figure 1a). Quantification of the fits (Figure 1b) reveals identical calcium incorporation in BG−CE and BG−CH as illustrated by similar amounts of Q^3_{Ca} and $Q^2_{Ca/H}$ species, the only difference being the lower degree of condensation (DC) of the silicate network when employing CE (78%) compared to CH (83%). On the contrary, the spectra of BG−CCl and BG−CCit correspond to pure depolymerized silica with only Q^4 and Q^3_H species observed, which means that calcium is not incorporated using $CaCl_2$ or calcium citrate even after adjusting the pH to 5, i.e., well above the IEP of silicic acid. As a conclusion, the pH alone does not explain the incorporation of calcium ions observed with CE and CH.

3.2. Mechanism of Calcium Incorporation. Based on these results, we propose the following reaction sequence to explain the incorporation of calcium into silicates using calcium alkoxide or CH in an acid catalyzed hydrolyzed silicate sol

$$Ca(OR)_2 = Ca^{2+} + 2\,RO^- \quad (2)$$

After its introduction in the sol, the $Ca(OR)_2$ precursor dissociates into Ca^{2+} and RO^- ions, which results in an increase of the pH. This increase mostly depends on the solubility of the calcium precursor in the solvent and the strength of the RO^- base.

$$Si{-}OH + RO^- = Si{-}O^- + ROH \quad (3)$$

The rise of the pH above the IEP of silicic acid shifts the acid−base equilibrium toward the formation of deprotonated silanols SiO^-, and the BG sol, which initially contained fully protonated silanols SiOH, now contains both SiO^- and SiOH. Additionally, we do not exclude the possibility of a heterogeneous acid−base reaction between the protonated silanols SiOH and the undissolved CE and CH powders, which would produce SiO^- and Ca^{2+} ions in a similar manner to eqs 2 and 3.

$$Si{-}O^- + Ca^{2+} \underset{\text{fast}}{\longrightarrow} Si{-}O^-\,{}^{+}Ca^{+} \quad (4)$$

An iono covalent bond is formed due to electrostatic attraction between SiO^- and Ca^{2+} ions. This might not happen in aqueous solutions if the molar ratio H_2O/TEOS ≫ 2, or with strongly polar solvents as the ions may be well stabilized by solvation. In fact, Ca^{2+} ions are known to be quickly released from BG upon immersion in water, while they remain in the BG upon immersion in absolute ethanol—which makes it an appropriate solvent for rinsing BG or BG−polymer hybrids.

$$Si{-}O^- + HO{-}Si \underset{\text{slow}}{\longrightarrow} Si{-}O{-}Si + HO^- \quad (5)$$

Concurrently with eq 4, the silicate network polymerizes. The condensation between silanol species occurs through a bimolecular nucleophilic substitution (S_N2) that is relatively slow compared to a simple electrostatic attraction; hence, eq 4 is thought to be favored over eq 5.

This mechanism is also supported by the discussions of Shah et al.,[35] Poologasundarampillai and Maçon,[31] and Ruiz Clavijo et al.[36] In this suggested reaction sequence, calcium incorporates through a unimolecular nucleophilic substitution (S_N1) type mechanism in which the rate determining step is fast (eq 2) and the second step is not really a nucleophilic attack, but rather an electrostatic attraction (eq 4). The removal of Ca^{2+} from solution as a result of the formation of $SiO^-\,{}^{+}Ca$ iono covalent bonds then promotes the dissociation of other $Ca(OR)_2$ molecules into Ca^{2+} and RO^- ions that will in turn react according to eqs 3 and 4. As suggested in the literature, $SiO^-\,{}^{+}Ca$ bonds may also form through a slower S_N2 type mechanism between the deprotonated silanols SiO^- and the undissolved CE and CH powders, better known as the condensation reaction in sol−gel chemistry.[5,13,18,19,21,22] In this

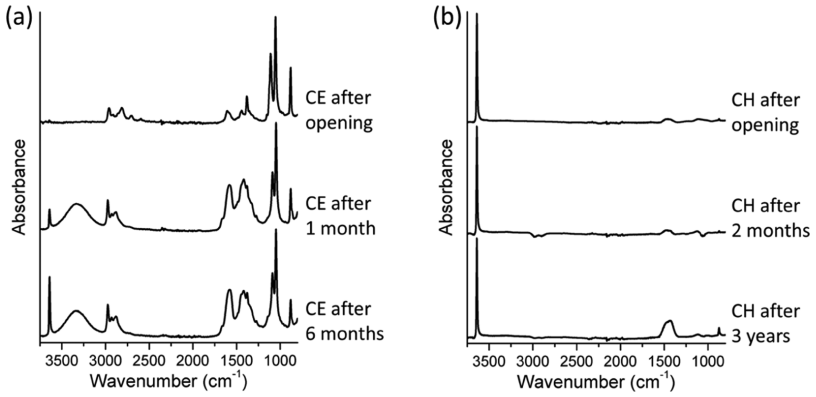

Figure 2. (a) Evolution of the ATR−FTIR spectrum of CE with storage time in argon. The spectra are normalized with respect to the narrow band at 1050 cm^{-1} (C−O stretching). Upon aging, CE hydrolyzes into CH as evidenced by the appearance of a sharp peak at 3640 cm^{-1} (O−H stretching). (b) Evolution of the ATR−FTIR spectrum of CH with storage time in air. The spectra are normalized with respect to the sharp peak at 3640 cm^{-1} (O−H stretching). Upon aging, calcium carbonates are formed as evidenced by the appearance of a broad band at 1430 cm^{-1} (CO_3^{2-} asymmetric stretching) and a sharp peak at 875 cm^{-1} (CO_3^{2-} out of plane bending).

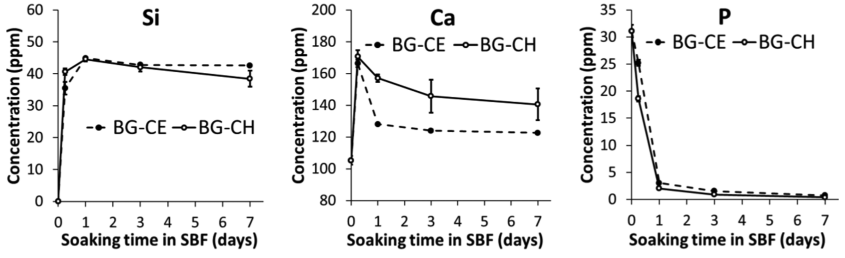

Figure 3. Evolution of Si, Ca, and P concentrations in simulated body fluid during the immersion of BG−CE and BG−CH powders (1 mL of SBF per mg of BG powder) as measured by ICP AES (n = 3). For BG−CE, standard deviations are mostly below 1 ppm.

way and despite the weak solubility of CE and CH in ethanol, we actually observe the CE and CH source powders to be progressively consumed in the silicate sol, reaching complete dissolution after approximately 30 min. This complete solubilization is never observed in a solution of pure ethanol. In parallel, the polymerization of the silicate network (eq 5) leads to the gelation of the sol after a time that depends on many parameters such as the pH, the concentration of reactive species, and the water to TEOS ratio.[34,37] Obviously, the gelation of the sol has to occur after the complete solubilization of the calcium source, which is the case here with our synthesis conditions.

With neutral salts like $CaCl_2$, the pH of the sol can still be increased above the IEP of silicic acid by adding a base (e.g., NaOH) to obtain SiO^- species. However, this still does not allow calcium incorporation. We suppose that the presence of the counterion (Cl^- here) prevents the formation of a SiO^- $^+$Ca bond. A similar behavior seems to be observed with NO_3^- as suggested by the study from Valliant et al., who found that calcium ions were not incorporated in silicates when using $Ca(NO_3)_2$ either at pH 1.4, 2.1, or 4.7.[40] Ideally, the counterion should be basic enough so that it can be eliminated through eq 3, like $C_2H_5O^-$ or HO^-, when using CE or CH, respectively. In this regard, weak bases like citrate may not be adequate counterions and calcium incorporation at low temperatures may only be possible by using strongly basic calcium sources like calcium alkoxides and CH.

3.3. Calcium Hydroxide as a Calcium Precursor. A reproducible gel time of the BG sol is required because it governs several physical properties of the resulting glass such as its degree of polymerization and the amount of residual alkoxy groups.[41] This is crucial for obtaining reproducible BG properties, a major requirement for translating the materials from bench to clinic but also when it comes to the synthesis of BG−polymer hybrids. Hybrid sols are commonly obtained by mixing a dissolved polymer with the BG sol right before its gelation so that the silicate network is well polymerized. When employing CE, the gelation of the acid catalyzed BG sol happens after a few hours to several days depending on the origin, age, and storage conditions of the calcium precursor, which complicates the synthesis of hybrids. This is why in the literature, a preferred solution is the "home made" synthesis of calcium alkoxides.[42] However, calcium alkoxides are prone to react with water, e.g., residual atmospheric humidity in the container, even when carefully stored in an inert atmosphere. As can be seen in Figure 2a, this hydrolysis reaction yields CH. As a result, the gel time of the BG−CE sol decreased from 2 h 40 min with a freshly opened CE (Gelest) to 1 h 30 min after several openings, which is the typical gel time measured for BG−CH sols (Table 1). Likewise, CH is known to progressively partially form CaO (upon dehydration)[43] and $CaCO_3$ (via carbonation)[44] under storage until a thermody namic equilibrium is reached. According to our experiments, the carbonation of CH is, however, very slow since its FTIR spectrum remains unchanged after 2 months of storage under ambient atmosphere (Figure 2b). As a result, the gel time of the BG−CH sols remained constantly equal to 1 h 30 min either with a freshly opened CH or with a 1 year old CH.

Therefore, CH allows reproducible syntheses and seems to be a rationale and attractive alternative to calcium alkoxides. To validate the relevance of CH as a calcium precursor, the apatite forming abilities of BG−CH and BG−CE were

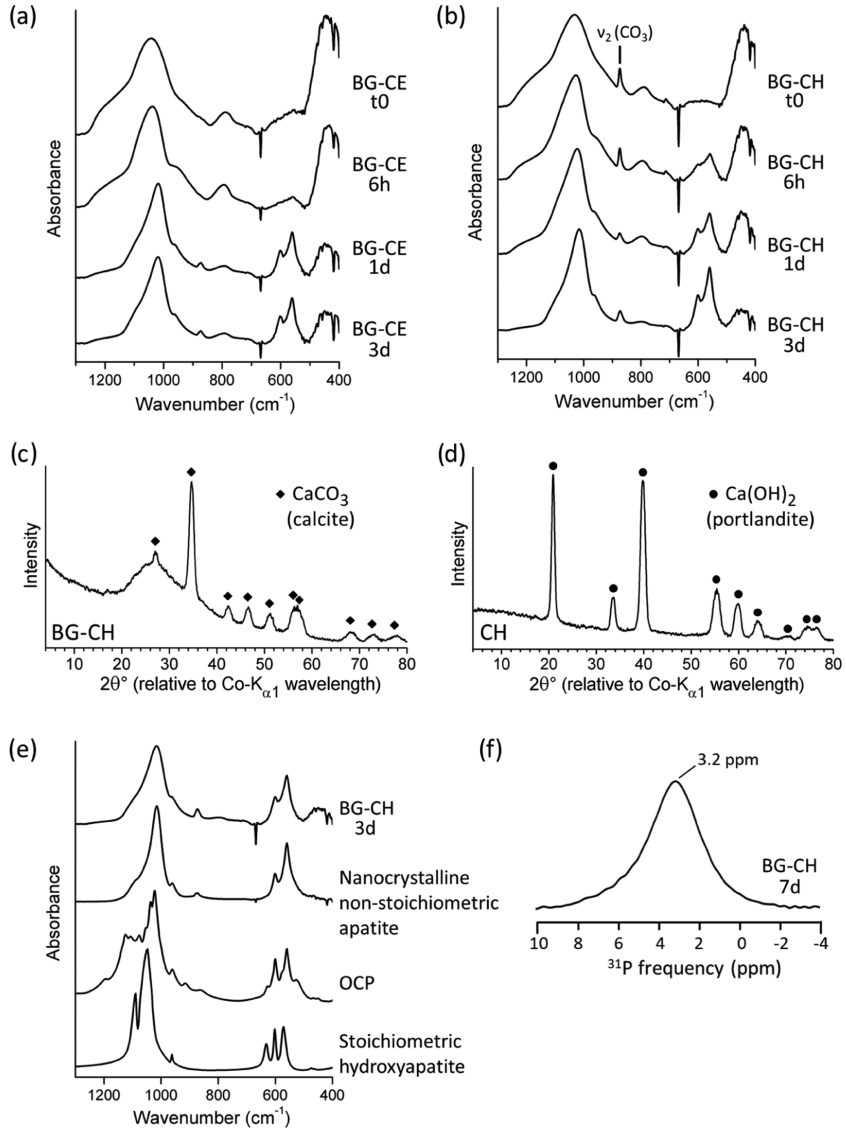

Figure 4. ATR−FTIR spectra of (a) BG−CE and (b) BG−CH before and after immersion in SBF for 6 h, 1 day, or 3 days. XRD patterns of (c) BG−CH and (d) CH; identified peaks correspond to calcite (file 01 086 2340 (PDF 2, 2004 database)) and portlandite (file 01 089 2779 (PDF 2, 2004 database)), respectively. (e) Comparison between the FTIR spectrum of BG−CH after 3 days of immersion in SBF and the characteristic FTIR spectra of various reference calcium phosphates. (f) Solid state ^{31}P MAS NMR spectrum of BG−CH after 7 days of immersion in SBF.

compared in vitro. The concentrations of Si, Ca, and P in SBF were monitored by ICP AES as a function of the BG soaking time. Figure 3 shows a similar trend for the two materials that is typical of BG interactions with SBF.[9] First, the glass dissolves and releases $SiO_x(OH)_{4-x}^{x-}$ and Ca^{2+} ions known to stimulate osteoblast proliferation and differentiation.[11,45,46] Calcium incorporation into the silicate network allows a smoother release[19] and its concentration in SBF only reaches approximately 170 ppm after 6 h of interaction, which is optimal for osteoblast proliferation and differentiation.[11] The ionic release changes the local supersaturation of the medium with regard to apatite formation[47] and triggers the precip itation of Ca^{2+} and HPO_4^{2-} ions (among others). Here, the precipitation of calcium phosphates seems slightly faster for BG−CH since less phosphorus is detected in SBF after 6 h of interaction (18.6 ± 0.5 ppm) compared to BG−CE (25.2 ± 0.6 ppm). This is correlated with the stronger calcium release observed for BG−CH, which favors apatite precipitation through higher supersaturation of the solution.

The chemical transformation of the materials was also characterized by FTIR spectroscopy (Figure 4a,b). FTIR spectra of the initial BG powders indicate the presence of carbonates when employing CH (Figure 4b), which is further confirmed by XRD as calcite $CaCO_3$ is found in BG−CH (Figure 4c). Yet, calcite was not detected in the XRD pattern of the raw CH precursor even after one year of aging (Figure 4d), meaning that it probably formed in situ during the synthesis of the BG sol following the reaction

$$Ca(OH)_2 + CO_2 \rightarrow CaCO_3 + H_2O \quad (6)$$

This atmospheric carbonation commonly arises during sol−gel preparations of calcium silicates under alkaline conditions[36,48] and may be avoided by carrying out the synthesis under an inert atmosphere. In contrast, when using CE as the calcium source, no carbonates are detected in the glass (Figure 4a), thereby suggesting that CE does not hydrolyze into CH during the sol−gel process. Besides the absorption band at 874 cm^{-1} assigned to the vibration of carbonates (CO_3^{2-} out of plane

bending, $v_2(CO_3)$) comprised in BG−CH, the FTIR spectra of the unreacted BG−CH and BG−CE powders are typical of sol−gel silicate glasses with bands located at 400−490 cm^{-1} (Si−O−Si rocking), 792 cm^{-1} (Si−O−Si bending), and 1000−1300 cm^{-1} (Si−O−Si asymmetric stretching), with a broad shoulder centered around 930 cm^{-1} (Si−OH stretching).[49,50] These vibrational contributions weaken with increasing time of interaction with SBF as a result of the depolymerization of the silicate network and the release of carbonates. New bands appear upon precipitation of calcium phosphates at the BG surface. No significant differences are observed here between BG−CH and BG−CE, therefore confirming their comparable dissolution rates and calcium phosphate forming abilities previously observed by ICP AES. Figure 4e displays characteristic FTIR spectra of various relevant calcium phosphates. After 3 days of immersion in SBF, the spectra of BG−CH and BG−CE nicely fit that of nanocrystalline nonstoichiometric apatite, as depicted by similar features, especially in the ν_4 (PO_4) region (ranging from 500 to 650 cm^{-1}) and the ν_3 (PO_4) region (ranging from 900 to 1200 cm^{-1}), as well as the ν_1 (PO_4) band at 964 cm^{-1} (P−O stretching) and the thin band at 873 cm^{-1} that could arise from apatitic HPO_4^{2-} ions (P−OH stretching) or apatitic CO_3^{2-} ions (CO_3^{2-} out of plane bending).[51] Solid state ^{31}P MAS NMR spectroscopy further confirms the apatitic nature of the newly formed calcium phosphate. The ^{31}P MAS NMR spectrum of BG−CH immersed for 7 days in SBF takes the form of a dissymmetric peak with a maximum around 3.2 ppm (Figure 4f) that distinctly corresponds to dried nanocrystalline apatite.[52] All of these data demonstrate the apatite forming ability of BG−CH.

The ultimate purpose of this study, thanks to a better understanding of the mechanism of calcium incorporation, was to identify a new and reliable calcium precursor (potentially CH) for the synthesis of BG−polymer hybrids. Therefore, as a validation step, organic−inorganic hybrid scaffolds based on SiO_2−CaO BG and PCL were fabricated using CH (PCL−CH) or CE (PCL−CE) as calcium precursors following a sol−gel process that was described in a previous work.[22] The physicochemical properties of PCL−CH and PCL−CE were compared. First of all, regarding the obtained macroporous structures, PCL−CH and PCL−CE are very similar, with well defined pores and many interconnections (Figure 5a). The porogen leaching method efficiently introduces porosity at ambient temperature, but it involves multiple washing steps to dissolve the porogen, so the successful and stable incorporation of calcium into the silicate network is a major concern here.[53] ^{29}Si MAS NMR spectroscopy on PCL−CH confirms that calcium ions entered the silicate network of the hybrid (Figure 5b), with the presence of signature Q^3_{Ca} and $Q^2_{Ca/H}$ units, thus demonstrating the sustainability of the calcium incorporation even after multiple baths. FTIR spectra of PCL−CE and PCL−CH (Figure 5c) are very similar and combine the characteristics of PCL and BG. The presence of carbonates is detected in PCL−CH. Upon immersion in SBF, the inorganic phase of the hybrids dissolves while calcium phosphates are formed. Figure 6a,b shows that this occurs at similar rates for PCL−CH and PCL−CE. After 7 days of soaking in SBF, the ν_4 (PO_4) region ranging from 500 to 650 cm^{-1} in the FTIR spectra of the hybrid scaffolds suggests the presence of nanocrystalline apatite (Figure 6c), although some other characteristic features of nanocrystalline apatite (detailed previously) are overlapped by absorption peaks arising from

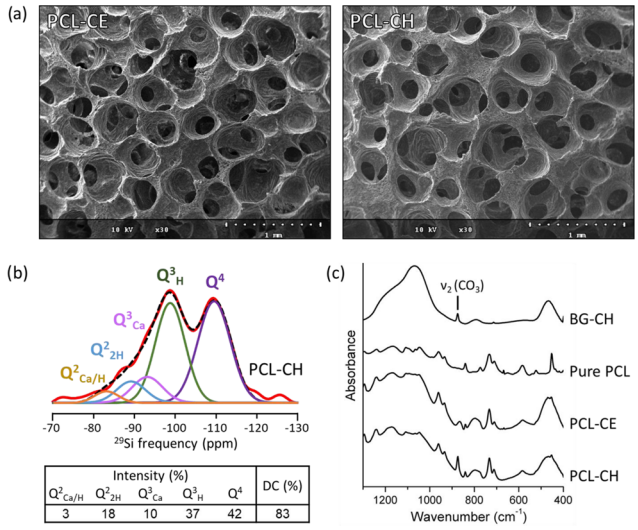

Figure 5. Structural characterization of BG−PCL hybrid scaffolds. (a) Representative SEM images of PCL−CE and PCL−CH scaffolds. (b) Experimental solid state ^{29}Si MAS NMR spectrum (red line) of PCL−CH scaffold and its fit (black dots). Individual Q^n contributions are shown below the experimental spectrum. Table shows relative intensities of Q^n resonances obtained from fits and degree of condensation (DC). The presence of Q^3_{Ca} and $Q^2_{Ca/H}$ species demonstrates the incorporation of calcium ions in the silicate network of the hybrid. (c) Transmission FTIR spectra of BG−CH, pure PCL, PCL−CE scaffold, and PCL−CH scaffold.

PCL. The XRD pattern of PCL−CH immersed for 7 days in SBF (Figure 6d) exhibits emerging peaks at 2θ angles of approximately 30 and 37° corresponding to the (002) and (211) lines of apatite, respectively.[54] While the XRD pattern of octacalcium phosphate (OCP) also features these peaks, OCP is also characterized by a distinctive peak at $2\theta \sim 6°$ (reflection on the (100) planes of OCP)[51] that is not detected here. Moreover, SEM observation of precipitates formed on PCL−CH after 7 days reveals the typical spherulitic morphology of growing apatite crystals (Figure 6e). Taken together, these data demonstrate the ability of PCL−CH hybrid scaffolds to form bone like minerals in vitro. Finally, the cytotoxicity of the samples was evaluated. Primary osteoblasts were cultured in the presence of preconditioned PCL−CH, preconditioned PCL−CE, or without material for the control condition and the cell viability was determined after 6 days. Figure 7 demonstrates that the dissolution products of the hybrids are noncytotoxic, given that no statistical difference is observed with the control conditions.

4. CONCLUSIONS

In this work, we have deepened the understanding of the mechanism of calcium incorporation inside silicates during the acid−base catalyzed sol−gel synthesis of BG. The basic property of the calcium precursor plays an essential role in the mechanism of calcium incorporation as the increase of the pH above the IEP of silicic acid leads to the deprotonation of silanols. The SiO^- anions then form iono covalent bonds with Ca^{2+} cations through electrostatic attraction. Here, the nature of the Ca^{2+} counterion in the calcium source plays a major role and explains why calcium salts like $CaCl_2$ and $Ca(NO_3)_2$ cannot lead to calcium incorporation, contrary to calcium alkoxides and CH. Thanks to our better understanding of the reaction sequence leading to calcium incorporation, we have

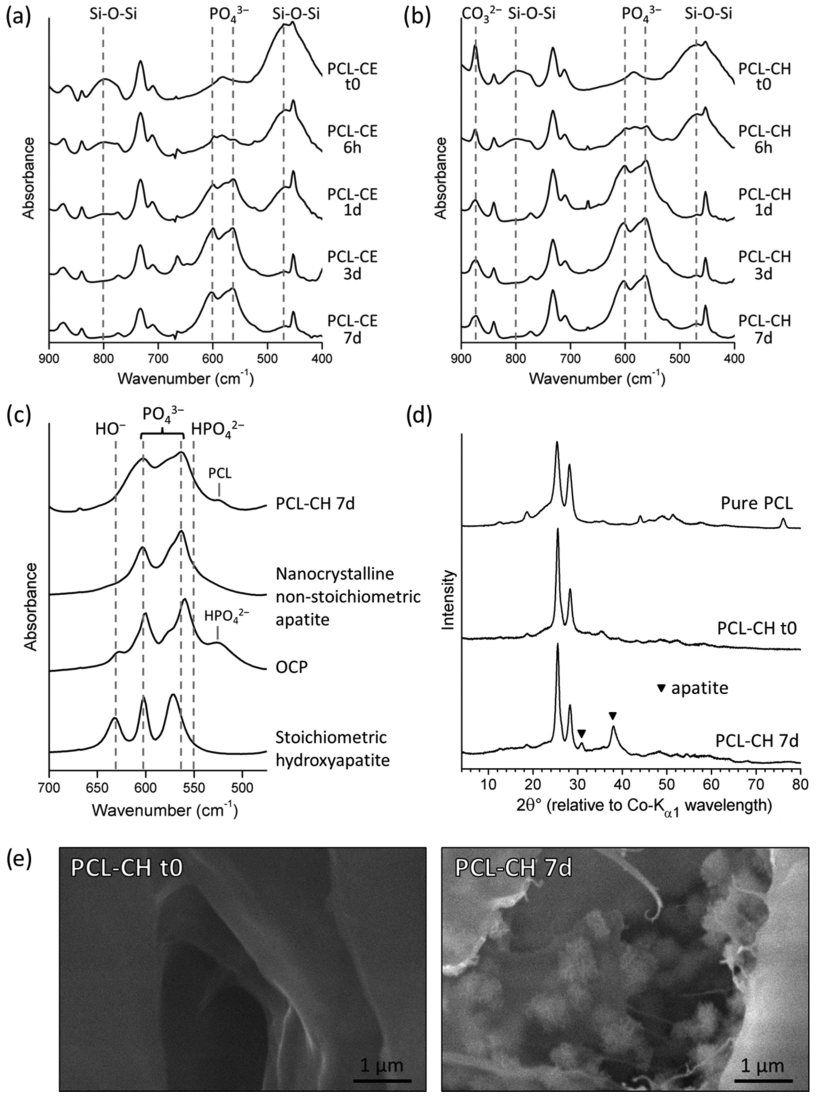

Figure 6. Evaluation of the apatite forming ability of BG−PCL hybrid scaffolds. Transmission FTIR spectra of (a) PCL−CE and (b) PCL−CH scaffolds before and after immersion in SBF for 6 h, 1 day, 3 days, or 7 days. (c) Comparison between the FTIR spectrum of the PCL−CH scaffold after 7 days of immersion in SBF and the characteristic FTIR spectra of various calcium phosphates. (d) XRD patterns of pure PCL and PCL−CH scaffold before and after 7 days of immersion in SBF. Identified peaks correspond to apatite (file 01 084 1998 (PDF 2, 2004 database)). (e) Representative SEM images of the surface of PCL−CH scaffolds before and after 7 days of immersion in SBF. Crystals were found to nucleate preferentially in the micrometric pores that resulted from the degradation of the material.

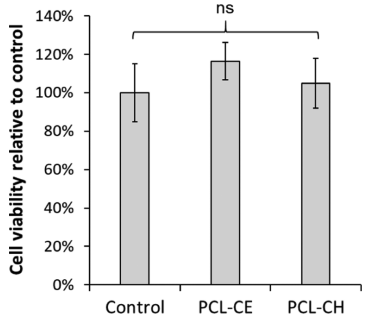

Figure 7. Cell viability of primary osteoblasts cultured for 6 days in the presence of preconditioned PCL−CE and PCL−CH scaffolds compared to the control condition (no scaffold), $n = 3$. Differences between samples were estimated using Tukey's HSD post hoc test (significance level was set to 0.05, ns = nonsignificant).

been able to use CH as an alternative to calcium alkoxides for the sol−gel synthesis of BG and BG−polymer hybrids at room temperature. Using CH yields several key advantages over calcium alkoxides, such as the low price and commercial availability of the calcium source, but more importantly, reproducible gelation times were obtained for the synthesis of BG−CH, while for BG−CE, it was highly dependent on the age, batch, and supplier of the CE used. The gel time of the BG sol is an important parameter in the synthesis of BG−polymer hybrids and this increase in reproducibility is therefore a significant step toward the industrialization of the process. Moreover, employing CH instead of CE did not alter the apatite forming ability of both BG and BG−PCL hybrids, or the interconnected macroporous structure of BG−PCL hybrid scaffolds. The proposed mechanism for calcium incorporation into silicates might also be applied to describe the incorporation of other alkaline or alkaline earth elements; for instance, pilot studies indicate that strontium hydroxide allows

the incorporation of strontium ions into the silicate network of acid–base catalyzed BG at room temperature in a similar manner to strontium alkoxides.

AUTHOR INFORMATION

Corresponding Author

*E mail: cedric.bossard@clermont.in2p3.fr.

ORCID

Cédric Bossard: 0000 0002 7892 1382

Henri Granel: 0000 0003 0898 4924

Christophe Drouet: 0000 0002 8471 8719

Notes

The authors declare no competing financial interest.

ACKNOWLEDGMENTS

The project was supported by the "Fonds Européen de Développement Régional" (FEDER). The Conseil Régional d'Auvergne is acknowledged for funding. Dr Mhammed Benbakkar and the Laboratoire Magma et Volcans (UMR 6524, CNRS/Université Blaise Pascal) are acknowledged for ICP AES measurements.

REFERENCES

(1) Hench, L. L. The story of Bioglass. *J. Mater. Sci.: Mater. Med.* 2006, *17*, 967–978.

(2) Hench, L. L.; Paschall, H. A. Direct chemical bond of bioactive glass ceramic materials to bone and muscle. *J. Biomed. Mater. Res.* 1973, *7*, 25–42.

(3) Xynos, I. D.; Edgar, A. J.; Buttery, L. D. K.; Hench, L. L.; Polak, J. M. Gene expression profiling of human osteoblasts following treatment with the ionic products of Bioglass 45S5 dissolution. *J. Biomed. Mater. Res.* 2001, *55*, 151–157.

(4) Fu, Q.; Saiz, E.; Rahaman, M. N.; Tomsia, A. P. Bioactive glass scaffolds for bone tissue engineering: state of the art and future perspectives. *Mater. Sci. Eng., C* 2011, *31*, 1245–1256.

(5) Jones, J. R. Review of bioactive glass: from Hench to hybrids. *Acta Biomater.* 2013, *9*, 4457–4486.

(6) Mahony, O.; Tsigkou, O.; Ionescu, C.; Minelli, C.; Ling, L.; Hanly, R.; Smith, M. E.; Stevens, M. M.; Jones, J. R. Silica gelatin hybrids with tailorable degradation and mechanical properties for tissue regeneration. *Adv. Funct. Mater.* 2010, *20*, 3835–3845.

(7) Kascholke, C.; Hendrikx, S.; Flath, T.; Kuzmenka, D.; Dörfler, H. M.; Schumann, D.; Gressenbuch, M.; Schulze, F. P.; Schulz Siegmund, M.; Hacker, M. C. Biodegradable and adjustable sol gel glass based hybrid scaffolds from multi armed oligomeric building blocks. *Acta Biomater.* 2017, *63*, 336–349.

(8) Mondal, D.; Lin, S.; Rizkalla, A. S.; Mequanint, K. Porous and biodegradable polycaprolactone borophosphosilicate hybrid scaffolds for osteoblast infiltration and stem cell differentiation. *J. Mech. Behav. Biomed. Mater.* 2019, *92*, 162–171.

(9) Ohtsuki, C.; Kokubo, T.; Yamamuro, T. Mechanism of apatite formation on CaO SiO_2 P_2O_5 glasses in a simulated body fluid. *J. Non Cryst. Solids* 1992, *143*, 84–92.

(10) Romero Gavilán, F.; Araújo Gomes, N.; Cerqueira, A.; García Arnáez, I.; Martínez Ramos, C.; Azkargorta, M.; Iloro, I.; Elortza, F.; Gurruchaga, M.; Suay, J.; Goñi, I. Proteomic analysis of calcium enriched sol–gel biomaterials. *JBIC, J. Biol. Inorg. Chem.* 2019, 563–574.

(11) Maeno, S.; Niki, Y.; Matsumoto, H.; Morioka, H.; Yatabe, T.; Funayama, A.; Toyama, Y.; Taguchi, T.; Tanaka, J. The effect of calcium ion concentration on osteoblast viability, proliferation and differentiation in monolayer and 3D culture. *Biomaterials* 2005, *26*, 4847–4855.

(12) Lin, S.; Ionescu, C.; Pike, K. J.; Smith, M. E.; Jones, J. R. Nanostructure evolution and calcium distribution in sol gel derived bioactive glass. *J. Mater. Chem.* 2009, *19*, 1276–1282.

(13) Yu, B.; Turdean Ionescu, C. A.; Martin, R. A.; Newport, R. J.; Hanna, J. V.; Smith, M. E.; Jones, J. R. Effect of calcium source on structure and properties of sol gel derived bioactive glasses. *Langmuir* 2012, *28*, 17465–17476.

(14) Pereira, M. M.; Jones, J. R.; Hench, L. L. Bioactive glass and hybrid scaffolds prepared by sol–gel method for bone tissue engineering. *Adv. Appl. Ceram.* 2005, *104*, 35–42.

(15) Allo, B. A.; Rizkalla, A. S.; Mequanint, K. Synthesis and electrospinning of polycaprolactone bioactive glass hybrid biomate rials via a sol–gel process. *Langmuir* 2010, *26*, 18340–18348.

(16) Ding, Y.; Roether, J. A.; Boccaccini, A. R.; Schubert, D. W. Fabrication of electrospun poly (3 hydroxybutyrate)/poly (e caprolactone)/silica hybrid fibermats with and without calcium addition. *Eur. Polym. J.* 2014, *55*, 222–234.

(17) Rámila, A.; Balas, F.; Vallet Regí, M. Synthesis routes for bioactive sol gel glasses: alkoxides versus nitrates. *Chem. Mater.* 2002, *14*, 542–548.

(18) Poologasundarampillai, G.; Yu, B.; Jones, J. R.; Kasuga, T. Electrospun silica/PLLA hybrid materials for skeletal regeneration. *Soft Matter* 2011, *7*, 10241–10251.

(19) Poologasundarampillai, G.; Yu, B.; Tsigkou, O.; Wang, D.; Romer, F.; Bhakhri, V.; Giuliani, F.; Stevens, M. M.; McPhail, D. S.; Smith, M. E.; Hanna, J. V.; Jones, J. R. PGA/silica hybrids with calcium incorporated in the silica network by use of a calcium alkoxide precursor. *Chem. Eur. J.* 2014, *20*, 8149–8160.

(20) Li, A.; Shen, H.; Ren, H.; Wang, C.; Wu, D.; Martin, R. A.; Qiu, D. Bioactive organic/inorganic hybrids with improved mechanical performance. *J. Mater. Chem. B* 2015, *3*, 1379–1390.

(21) Lao, J.; Dieudonne, X.; Fayon, F.; Montouillout, V.; Jallot, E. Bioactive glass gelatin hybrids: building scaffolds with enhanced calcium incorporation and controlled porosity for bone regeneration. *J. Mater. Chem. B* 2016, *4*, 2486–2497.

(22) Bossard, C.; Granel, H.; Jallot, É.; Vial, C.; Tiainen, H.; Wittrant, Y.; Lao, J. Polycaprolactone / bioactive glass hybrid scaffolds for bone regeneration. *Biomed. Glasses* 2018, *4*, 108–122.

(23) Granel, H.; Bossard, C.; Collignon, A. M.; Wauquier, F.; Lesieur, J.; Rochefort, G. Y.; Jallot, E.; Lao, J.; Wittrant, Y. Bioactive glass/polycaprolactone hybrid with a dual cortical/trabecular structure for bone regeneration. *ACS Appl. Bio Mater.* 2019, 3473.

(24) Sepulveda, P.; Jones, J. R.; Hench, L. L. Bioactive sol gel foams for tissue repair. *J. Biomed. Mater. Res.* 2002, *59*, 340–348.

(25) Vandecandelaere, N.; Rey, C.; Drouet, C. Biomimetic apatite based biomaterials: on the critical impact of synthesis and post synthesis parameters. *J. Mater. Sci.: Mater. Med.* 2012, *23*, 2593–2606.

(26) Bohner, M.; Lemaitre, J. Can bioactivity be tested in vitro with SBF solution? *Biomaterials* 2009, *30*, 2175–2179.

(27) Fung, B. M.; Khitrin, A. K.; Ermolaev, K. An improved broadband decoupling sequence for liquid crystals and solids. *J. Magn. Reson.* 2000, *142*, 97–101.

(28) Massiot, D.; Fayon, F.; Capron, M.; King, I.; Le Calvé, S.; Alonso, B.; Durand, J. O.; Bujoli, B.; Gan, Z.; Hoatson, G. Modelling one and two dimensional solid state NMR spectra. *Magn. Reson. Chem.* 2002, *40*, 70–76.

(29) Declercq, H.; Van den Vreken, N.; De Maeyer, E.; Verbeeck, R.; Schacht, E.; De Ridder, L.; Cornelissen, M. Isolation, proliferation and differentiation of osteoblastic cells to study cell/biomaterial interactions: comparison of different isolation techniques and source. *Biomaterials* 2004, *25*, 757–768.

(30) Midha, S.; Kim, T. B.; van den Bergh, W.; Lee, P. D.; Jones, J. R.; Mitchell, C. A. Preconditioned 70S30C bioactive glass foams promote osteogenesis in vivo. *Acta Biomater.* 2013, *9*, 9169–9182.

(31) Poologasundarampillai, G.; Maçon, A. L. B. Organic–Inorganic Hybrid Biomaterials. In *Bioactive Glasses: Fundamentals, Technology and Applications*; The Royal Society of Chemistry, 2017; pp 286–302.

(32) Iler, R. K. The chemistry of silica. *J. Chem. Educ.* 1980, *57*, No. A324.

(33) Maçon, A. L. B.; Jacquemin, M.; J. Page, S.; Li, S.; Bertazzo, S.; M. Stevens, M.; V. Hanna, J.; Jones, J. Lithium silicate sol gel

bioactive glass and the effect of lithium precursor on structure property relationships. *J. Sol Gel Sci. Technol.* **2017**, *81*, 84−94.
(34) Brinker, C. J.; Scherer, G. W. *Sol Gel Science: The Physics and Chemistry of Sol Gel Processing*; Academic Press, 1990.
(35) Shah, A. T.; Batool, M.; Chaudhry, A. A.; Iqbal, F.; Javaid, A.; Zahid, S.; Ilyas, K.; bin Qasim, S.; Khan, A. F.; Khan, A. S.; ur Rehman, I. Effect of calcium hydroxide on mechanical strength and biological properties of bioactive glass. *J. Mech. Behav. Biomed. Mater.* **2016**, *61*, 617−626.
(36) Ruiz Clavijo, A.; Hurt, P. A.; Kotha, K. A.; Coleman, J. N. Effect of calcium precursor on the bioactivity and biocompatibility of sol gel derived glasses. *J. Funct. Biomater.* **2019**, *10*, 13.
(37) Klein, L. C. Sol gel processing of silicates. *Annu. Rev. Mater. Sci.* **1985**, *15*, 227−248.
(38) Mondal, D.; Rizkalla, A. S.; Mequanint, K. Bioactive borophosphosilicate polycaprolactone hybrid biomaterials via a non aqueous sol gel process. *RSC Adv.* **2016**, *6*, 92824−92832.
(39) Fernando, D.; Attik, N.; Cresswell, M.; Mokbel, I.; Pradelle Plasse, N.; Jackson, P.; Grosgogeat, B.; Colon, P. Influence of network modifiers in an acetate based sol gel bioactive glass system. *Microporous Mesoporous Mater.* **2018**, *257*, 99−109.
(40) Valliant, E. M.; Turdean Ionescu, C. A.; Hanna, J. V.; Smith, M. E.; Jones, J. R. Role of pH and temperature on silica network formation and calcium incorporation into sol gel derived bioactive glasses. *J. Mater. Chem.* **2012**, *22*, 1613−1619.
(41) Brinker, C. J. Hydrolysis and condensation of silicates: Effects on structure. *J. Non Cryst. Solids* **1988**, *100*, 31−50.
(42) Liu, X.; Piao, X.; Wang, Y.; Zhu, S. Calcium ethoxide as a solid base catalyst for the transesterification of soybean oil to biodiesel. *Energy Fuels* **2008**, *22*, 1313−1317.
(43) Criado, Y. A.; Alonso, M.; Abanades, J. C. Kinetics of the CaO/$Ca(OH)_2$ hydration/dehydration reaction for thermochemical energy storage applications. *Ind. Eng. Chem. Res.* **2014**, *53*, 12594−12601.
(44) Montes Hernandez, G.; Chiriac, R.; Toche, F.; Renard, F. Gas solid carbonation of $Ca(OH)_2$ and CaO particles under non isothermal and isothermal conditions by using a thermogravimetric analyzer: Implications for CO_2 capture. *Int. J. Greenhouse Gas Control* **2012**, *11*, 172−180.
(45) Zou, S.; Ireland, D.; Brooks, R. A.; Rushton, N.; Best, S. The effects of silicate ions on human osteoblast adhesion, proliferation, and differentiation. *J. Biomed. Mater. Res., Part B* **2009**, *90*, 123−130.
(46) Kim, E. J.; Bu, S. Y.; Sung, M. K.; Choi, M. K. Effects of silicon on osteoblast activity and bone mineralization of MC3T3 E1 cells. *Biol. Trace Elem. Res.* **2013**, *152*, 105−112.
(47) Lu, X.; Leng, Y. Theoretical analysis of calcium phosphate precipitation in simulated body fluid. *Biomaterials* **2005**, *26*, 1097−1108.
(48) Luz, G. M.; Mano, J. F. Preparation and characterization of bioactive glass nanoparticles prepared by sol−gel for biomedical applications. *Nanotechnology* **2011**, *22*, No. 494014.
(49) Aguiar, H.; Serra, J.; González, P.; León, B. Structural study of sol gel silicate glasses by IR and Raman spectroscopies. *J. Non Cryst. Solids* **2009**, *355*, 475−480.
(50) Kalampounias, A. G. IR and Raman spectroscopic studies of sol gel derived alkaline earth silicate glasses. *Bull. Mater. Sci.* **2011**, *34*, 299−303.
(51) Drouet, C. Apatite formation: why it may not work as planned, and how to conclusively identify apatite compounds. *BioMed Res. Int.* **2013**, *2013*, 12.
(52) Eichert, D.; Sfihi, H.; Combes, C.; Rey, C. Specific characteristics of wet nanocrystalline apatites. Consequences on biomaterials and bone tissue. *Key Eng. Mater.* **2003**, *254−256*, 927−930.
(53) Hendrikx, S.; Kuzmenka, D.; Köferstein, R.; Flath, T.; Uhlig, H.; Enke, D.; Schulze, F. P.; Hacker, M. C.; Schulz Siegmund, M. Effects of curing and organic content on bioactivity and mechanical properties of hybrid sol−gel glass scaffolds made by indirect rapid prototyping. *J. Sol Gel Sci. Technol.* **2017**, *83*, 143−154.
(54) Grunenwald, A.; Keyser, C.; Sautereau, A. M.; Crubézy, E.; Ludes, B.; Drouet, C. Revisiting carbonate quantification in apatite (bio)minerals: a validated FTIR methodology. *J. Archaeol. Sci.* **2014**, *49*, 134−141.